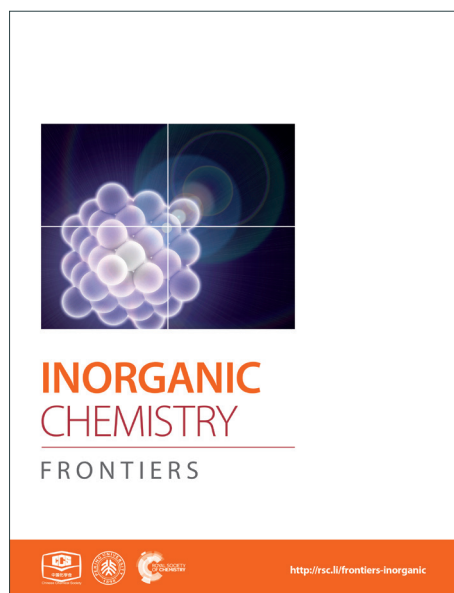
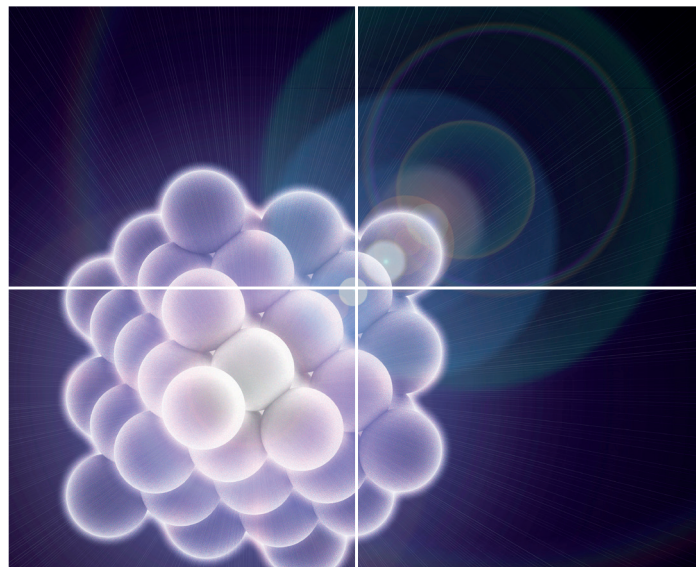


# INORGANIC CHEMISTRY

FRONTIERS

Accepted Manuscript



This is an *Accepted Manuscript*, which has been through the Royal Society of Chemistry peer review process and has been accepted for publication.

*Accepted Manuscripts* are published online shortly after acceptance, before technical editing, formatting and proof reading. Using this free service, authors can make their results available to the community, in citable form, before we publish the edited article. We will replace this *Accepted Manuscript* with the edited and formatted *Advance Article* as soon as it is available.

You can find more information about *Accepted Manuscripts* in the [Information for Authors](#).

Please note that technical editing may introduce minor changes to the text and/or graphics, which may alter content. The journal's standard [Terms & Conditions](#) and the [Ethical guidelines](#) still apply. In no event shall the Royal Society of Chemistry be held responsible for any errors or omissions in this *Accepted Manuscript* or any consequences arising from the use of any information it contains.

**Experimental and theoretical investigation of the magnetic and photoconductive nature of a novel two-dimensional, mixed-valence bis(2-thioxo-1, 3-dithiole-4, 5-dithiolato)-nickelate molecular solid**

Hao Yang,<sup>a</sup> Jian-Lan Liu,<sup>a</sup> Lan-Cheng Zhou,<sup>a</sup> and Xiao-Ming Ren<sup>\*a,b,c</sup>

<sup>a</sup> State Key Laboratory of Materials-Oriented Chemical Engineering and College of Science, Nanjing University of Technology, Nanjing 210009, People's Republic of China.

<sup>b</sup> College of Materials Science and Engineering, Nanjing University of Technology, Nanjing 210009, People's Republic of China.

<sup>c</sup> State Key Laboratory & Coordination Chemistry Institute, Nanjing University, Nanjing 210093, People's Republic of China.

Tel: +86 25 58139476

Fax: +86 25 58139481

E-mail: [xmren@njtech.edu.cn](mailto:xmren@njtech.edu.cn)

## Abstract

A two-dimensional, mixed-valence  $[\text{Ni}(\text{dmit})_2]$  compound,  $[\text{C}_8\text{-Apy}]_2[\text{Ni}(\text{dmit})_2]_3$  (**1**) (where  $\text{dmit}^{2-}$  = 2-thioxo-1,3-dithiole-4,5-dithiolate and  $\text{Apy}^+$  = 4-amino-1-alkylpyridinium) was prepared and its structure fully characterized. The molecular solid displays a layered structure along the crystallographic c-axis with a  $[\text{Ni}(\text{dmit})_2]$  layer constructed from alternating straight chains of  $[\text{Ni}(\text{dmit})_2]^0$  and two-legged ladder chains of  $[\text{Ni}(\text{dmit})_2]^{1-}$ . Compound **1** shows antiferromagnetic, spin-dimer with pairwise interaction magnetic behavior and semiconducting nature in addition to a rapid, clear and stable response of photoconductivity under UV irradiation. The magnetic coupling nature of **1** was analyzed using the ‘broken-symmetry’ density functional theory (DFT) approach. The electronic band structure was calculated using the CASTEP program and was used to investigate the theoretical transport and photoconductive behavior of **1**. This work suggests mixed-valence  $[\text{Ni}(\text{dmit})_2]$  compounds have great potential as the building blocks for new photoconductor based materials.

Keywords: Metal-dithiolene complex, mixed-valence, two-dimensional, photoconductivity, magnetism

## Introduction

The metal salt  $[M(\text{dmit})_2]$  ( $\text{dmit}^{2-} = 2\text{-thioxo-1,3-dithiole-4,5-dithiolate}$ ) displays an interesting molecular architecture, with its ten peripheral S atoms enabling a multidimensional electrical network *via* intermolecular S...S bonding interactions in the solid state.<sup>1</sup> The electronic structure and physical properties of these metal salts depend on the molecular arrangement of  $[M(\text{dmit})_2]$  in the solid state, which is also related to the shape and size of the metal counter ions present. Therefore, considerable research effort towards the development of  $[M(\text{dmit})_2]$  compounds with unique electronic structures and physical properties using rational design of the counter ion structure has been reported.<sup>1-5</sup> Nakamura and co-workers<sup>2</sup> reported the supramolecular M-crown ether cation (where M = alkaline metal ion, alkaline earth metal ion or organic ammonium ion) into the  $[\text{Ni}(\text{dmit})_2]$  system to give a molecular metal compound with  $\text{Li}^+$  ion conducting channels and a supramolecular rotator that achieved ferroelectricity and polarity control *via* a switching flip-flop motion of the rotator unit using an external electric field. Kusamoto and co-workers<sup>3</sup> reported the novel bilayer Mott salt, (ethyl-4-bromothiazolium) $[\text{Ni}(\text{dmit})_2]_2$ , in which the coexistence of antiferromagnetic (AFM) and ferromagnetic (FM) anionic layers displayed an unusual ferromagnetic anomaly and large negative magnetoresistance. Fourmigué and co-workers<sup>4</sup> prepared the first chiral, mixed-valence conducting  $[\text{Ni}(\text{dmit})_2]$  salt incorporating a chiral counter ion with an unusual 2:5 stoichiometry between the cationic counter ion and  $[\text{Ni}(\text{dmit})_2]$  units.

The conductivity of the  $[\text{Ni}(\text{dmit})_2]$  metal salts has been extensively studied and shows a diverse range of behavior from use as Mott insulators,<sup>6</sup> semi-conductors<sup>7</sup> to metal-like conductors.<sup>8</sup> However, investigation into the photoconductivity of  $[\text{Ni}(\text{dmit})_2]$  metal salts is limited.<sup>9</sup> There has been an ever-growing use of photodetectors in a wide range of everyday and high-end applications, for example, the use of UV-visible light photoconductors in environmentally-based detectors, space research and optical communications.<sup>10</sup>

Our research has involved the incorporation of flexible cations, such as 4-amino-1-alkylpyridinium ( $C_n\text{-Apy}^+$ ) to the  $[\text{Ni}(\text{dmit})_2]$  metal salt system in an effort to control the stacking pattern and physical properties. We now report the synthesis of a novel, two-dimensional mixed-valence  $[\text{Ni}(\text{dmit})_2]$  metal salt,  $[\text{C}_8\text{-Apy}]_2[\text{Ni}(\text{dmit})_2]_3$  (**1**), which displays an unusual 2:3 stoichiometry between  $\text{C}_8\text{-Apy}^+$  and  $[\text{Ni}(\text{dmit})_2]$ , in addition to a rapid, clear and stable response of photoconductivity under UV irradiation. The crystal structure, magnetism, conductivity and photoconductivity of **1** were also investigated.

## Experimental

### Materials

All chemicals and reagents were purchased from commercial sources and used with no further purification. 4, 5-di(thiobenzoyl)-1, 3-dithiole-2-thione was prepared according to the procedure reported by Steimecke et al.<sup>11</sup>  $[\text{C}_8\text{-Apy}]\text{Br}$  was prepared using the procedure reported for the synthesis of  $[\text{C}_6\text{-Apy}]\text{Br}$ .<sup>12</sup>

### Synthesis of $[\text{C}_8\text{-Apy}]_2[\text{Ni}(\text{dmit})_2]_3$ (**1**)

A suspension of 4, 5-di(thiobenzoyl)-1, 3-dithiole-2-thione (812 mg, 2.0 mmol) in methanol (10 mL) was added to a solution of sodium methoxide [prepared from sodium (184 mg, 8.0 mmol) in methanol (10 mL)] at room temperature under an atmosphere of argon. The reaction mixture was stirred at room temperature for 30 min resulting in a dark red solution.  $\text{NiCl}_2 \cdot 6\text{H}_2\text{O}$  (238 mg, 1.0 mmol), a solution of  $[\text{C}_8\text{-Apy}]\text{Br}$  (287 mg, 1.0 mmol) in methanol (20 mL) followed by a solution of  $\text{I}_2$  (127 mg, 0.5 mmol) and  $\text{NaI}$  (150 mg, 1.0 mmol) in methanol (20 mL) were added to the reaction mixture, the resulting mixture stirred at room temperature for 2 h and allowed to stand overnight (~16 h). The microcrystalline crude product was collected by filtration, washed with  $\text{MeOH}$  (20 mL) and dried *in vacuo*. The crude product was recrystallized from acetone to give the title compound **1** as dark green crystals with ca. 80% yield. Anal.Calc. for  $\text{C}_{44}\text{H}_{46}\text{N}_4\text{S}_{30}\text{Ni}_3$ : C, 29.88; H, 2.62; N, 3.17%. Found: C, 29.85; H, 2.77; N, 3.01%. IR

(KBr disc,)  $\nu = 1367, 1323 (\nu_{C=C}), 1068, 1054 (\nu_{C=S}), 514, 499 (\delta_{S-C-S}) \text{ cm}^{-1}$ . It is noted that the oxidation of ostensibly 1 mmol of  $[\text{Ni}(\text{dmit})_2]^{2-}$  into  $[\text{Ni}(\text{dmit})_2]^{2/3-}$  requires theoretically 1.33 "electron-equivalents" of the oxidant. Even accounting for the "only" 80% yield, this would have required  $> 0.5$  mmol of  $\text{I}_2$ , however, only 0.5 mmol of  $\text{I}_2$  (i.e., 1 mmol of oxidant "electron-equivalents") was used in the preparation procedure. Such a stoichiometric discrepancy is due to the overoxidation by air.

### Physical Measurements

Elemental analyses (C, H and N) were performed using a Vario EL III elemental analyzer. Powder X-ray diffraction (PXRD) data were collected using a Bruker D8 Advance powder diffractometer with Cu  $K\alpha$  radiation ( $\lambda = 1.5418 \text{ \AA}$ ). FT-IR spectra were recorded using a IF66 V FT-IR ( $4000\text{--}400 \text{ cm}^{-1}$ ) spectrophotometer on KBr discs. Magnetic susceptibility data were measured for polycrystalline samples using a Quantum Design MPMS-5S superconducting quantum interference device (SQUID) magnetometer over a temperature range of 1.8–400 K. Electrical conductivity measurements were made using a Keithley 2440 5A SourceMeter for the compressed powder pellet using a two-probe method. Photoconductivity was measured for a single crystal using a Zahner Zennium IM6 Electrochemical Workstation. The photocurrent  $I$  response to UV irradiation ( $\lambda = 375 \text{ nm}$ ; 3.3 eV) was measured using a needle-shaped single crystal at room temperature and two gold wires with a diameter of 80  $\mu\text{m}$  attached on the two opposite surfaces of the cross section of the needle crystal.

### X-Ray single crystallography

Single crystal X-ray diffraction data was collected using a Bruker Smart Apex II CCD detector with graphite-monochromated Mo  $K\alpha$  radiation ( $\lambda = 0.71073 \text{ \AA}$ ) at 296 K using the  $\omega$ -scan technique. Data was integrated using the SAINT program and subsequently used for the intensity corrections of the Lorentz and polarization effects. An empirical absorption correction was applied using the SADABS program.<sup>13</sup> The structure was solved by direct methods and all non-hydrogen atoms were

anisotropically refined on  $F^2$  by the full-matrix least-squares technique using the SHELXL-97 crystallographic software package.<sup>14</sup> All hydrogen atoms were placed at the calculated positions and refined as riding on the parent atoms. The experimental details for data collection, structure refinement and crystallography are summarized in **Table 1**.

**Table 1** Crystallographic data and refinement parameter for compound **1**

Temp. (K)	296(2)
Wavelength (Å)	0.71073
Formula	C <sub>44</sub> H <sub>46</sub> N <sub>4</sub> S <sub>30</sub> Ni <sub>3</sub>
Formula weight	1769.02
Space group	<i>P</i> -1
CCDC no.	956073
Crystal system	Triclinic
<i>a</i> (Å)	11.6986(12)
<i>b</i> (Å)	12.1197(12)
<i>c</i> (Å)	14.0622(14)
$\alpha$ (°)	109.910(3)
$\beta$ (°)	105.249(3)
$\gamma$ (°)	103.361(3)
<i>V</i> (Å <sup>3</sup> , Z)	1691.9(3)/1
$\rho$ (g cm <sup>-3</sup> )	1.736
$\mu$ (mm <sup>-1</sup> )	1.790
<i>F</i> (000)	902
$\theta$ Range for data collection (°)	1.92–27.55
	–15 ≤ <i>h</i> ≤ 15
Index ranges	–15 ≤ <i>k</i> ≤ 15
	–18 ≤ <i>l</i> ≤ 18
<i>R</i> <sub>int</sub>	0.0452
Independent reflect. / restraints / parameters	7788/0/369
Refinement method	The least square refinement on $F^2$
Goodness-of-fit on $F^2$	1.052
<i>R</i> <sub>1</sub> , <i>wR</i> <sub>2</sub> [ <i>I</i> > 2σ( <i>I</i> )] <sup>a</sup>	0.0423, 0.0760
<i>R</i> <sub>1</sub> , <i>wR</i> <sub>2</sub> [all data] <sup>a</sup>	0.0827, 0.0894
Residual (e Å <sup>-3</sup> )	0.337/–0.424

<sup>a</sup>  $R_1 = \sum ||F_o| - |F_c||/|F_o|$  and  $wR_2 = [\sum w(\sum F_o^2 - F_c^2)^2 / \sum w(F_o^2)^2]^{1/2}$ .

## Density functional theory (DFT) calculations for magnetic coupling constants and electronic band structures

All DFT calculations for magnetic coupling constants were carried out using the Gaussian09 program.<sup>15</sup> The single point energies of the high-spin triplet and the low-spin broken-symmetric states for the  $[\text{Ni}(\text{dmit})_2]_2^{2-}$  spin dimer or  $[\text{Ni}(\text{dmit})_2]_3^{2-}$  sandwich trimer present in compound **1** were calculated using the DFT approach on the non-modelized molecular geometry obtained from our X-ray single crystal structure analysis (the spin coupling interaction is sensitive to any changes in molecular structure, therefore no simplification or optimization of the molecular structure was made in our calculations). The popular hybrid exchange-correlation functional B3LYP, was composed of the Becke's three-parameter hybrid exchange functional,<sup>16</sup> LYP correlation functional<sup>17</sup> and lanl2dz relativistic effective core potential basis set<sup>18</sup> for the Ni elemental and 6-311+g(d,p) basis set for C, S elements used in our calculations. The SCF convergence criterion was  $10^{-8}$ .

Electronic band structure calculations were performed using the CASTEP program<sup>19</sup> for compound **1** on the non-modelized crystal structure obtained from our X-ray single crystal structure analysis. The cations in the crystal structure were removed in the calculations since the conductivity of this molecular solid is related to the anionic  $[\text{Ni}(\text{dmit})_2]^-$  and neutral  $[\text{Ni}(\text{dmit})_2]^0$  species. The generalized gradient approximation (GGA) of the Perdew–Burke–Ernzerhof (PBE)<sup>20</sup> potentials have been incorporated in our calculations. The k-points sampling in the Brillouin zone were set at  $4 \times 4 \times 3$  according to the Monkhorst–Pack scheme.<sup>21</sup> For all relevant calculations the plane wave basis set cut-off was fixed at 240 eV and the convergence criterion fixed at  $1.0 \times 10^{-5}$  eV/atom. The other calculating parameters were set at the default values in the CASTEP code.

## Results and discussion

### Crystal structure

$[\text{C}_8\text{-APy}]_2[\text{Ni}(\text{dmit})_2]_3$  (**1**) crystallizes in the triclinic space group  $P-1$ . An asymmetric unit was comprised of one  $\text{C}_8\text{-APy}^+$  cation together with one and a half planar  $[\text{Ni}(\text{dmit})_2]$  units (Figure 1a). The bond lengths and angles observed in the  $\text{C}_8\text{-APy}^+$  cation are within that expected. All atoms are located in the general positions of the  $[\text{Ni}(\text{dmit})_2]$  moiety containing Ni(1), whilst the Ni(2) atoms coincide with an inversion center to give a corresponding  $[\text{Ni}(\text{dmit})_2]$  moiety with  $C_i$  symmetry. The typical bond lengths observed in the two different  $[\text{Ni}(\text{dmit})_2]$  moieties are summarized in Table S1. The total charge of one and a half  $[\text{Ni}(\text{dmit})_2]$  moieties is  $-1$  because the  $\text{C}_8\text{-APy}^+$  cation has a  $+1$  charge. Therefore, the average oxidation state of the  $[\text{Ni}(\text{dmit})_2]$  moieties in the asymmetric unit is  $-2/3$ . The theoretical analysis based on DFT calculations at the b3lyp/lanl2dz level of theory predicted that the lowest unoccupied molecule orbital (LUMO) of the neutral complex  $[\text{Ni}(\text{dmit})_2]^0$  consists of the  $3d$  orbitals of Ni and the  $\pi$  (C=C) orbital of ligand (Figure 1b). In the anionic complex  $[\text{Ni}(\text{dmit})_2]^{1-}$ , the LUMO is bonding with respect to the  $\pi(\text{C}=\text{C})$  bond and antibonding with respect to the  $\sigma(\text{C}-\text{S})$  and  $\sigma(\text{Ni}-\text{S})$  bonds. The addition of one electron to the LUMO was expected to strengthen the  $\pi(\text{C}=\text{C})$  bond and weaken the  $\sigma(\text{C}-\text{S})$  and  $\sigma(\text{Ni}-\text{S})$  bonds. As a result, the bond distance of the  $\pi(\text{C}=\text{C})$  bond is reduced and the bond distances of both  $\sigma(\text{C}-\text{S})$  and  $\sigma(\text{Ni}-\text{S})$  bonds are increased with increasing  $n$  value in the series  $[\text{Ni}(\text{dmit})_2]^{n-}$  ( $n = 0, 1$  and  $2$ ). Upon careful analysis of the  $\pi(\text{C}=\text{C})$ ,  $\sigma(\text{C}-\text{S})$  and  $\sigma(\text{Ni}-\text{S})$  bond distances in compound **1**, we can conclude that the  $[\text{Ni}(\text{dmit})_2]$  moiety containing Ni(2) is a neutral species and the  $[\text{Ni}(\text{dmit})_2]$  moiety containing Ni(1) has a  $-1$  charge (Table S1). The assignments for Ni(1) and Ni(2) in compound **1** was further confirmed by (1) IR spectra analysis (Table S2 and Figure S2 where the vibration bands of  $\nu_{\text{C}=\text{C}}$ ,  $\nu_{\text{C}=\text{S}}$  and  $\nu_{\text{C}-\text{S}}$  contributed from both  $[\text{Ni}(\text{dmit})_2]^{1-}$  and  $[\text{Ni}(\text{dmit})_2]^0$  species are observed, respectively) and (2) the energy band structure calculation (see Figure S4, where the two band structures with different situations, namely, presence/absence of neutral  $[\text{Ni}(\text{dmit})_2]$  molecule (with Ni(2)), are shown, and

the comparison between two band structures provided the information about the inhomogeneity of the valence state between the three molecules in a trimer).

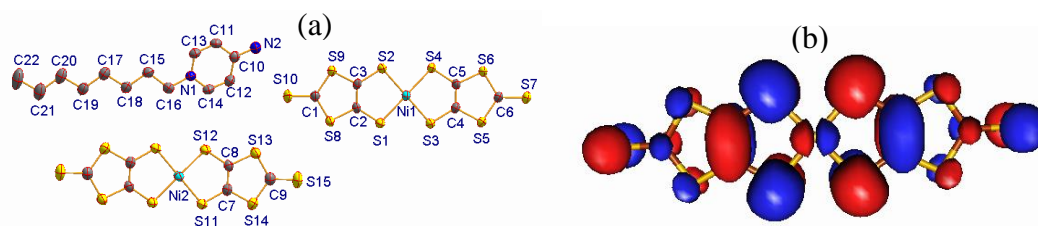


**Figure 1** (a) Molecular structure of compound **1** with all non-hydrogen atoms labeled. (b) LUMO of neutral  $[\text{Ni}(\text{dmit})_2]^0$  obtained from DFT calculations at the B3LYP/lanl2dz level of theory.

The  $\text{C}_8\text{-APy}^+$  cation and the mixed-valence  $[\text{Ni}(\text{dmit})_2]$  species form alternating layers along the crystallographic  $c$ -axis direction as shown in **Figure 2a**. The neighboring cations adopt a parallel arrangement along  $b$ -axis direction and an anti-parallel alignment along the  $a$ -axis direction (**Figure 2b**) within the cationic layer. The anionic layer is constructed of the  $\pi$ -type anion trimers adopting an alignment in the  $[\text{Ni}(\text{dmit})_2]^{1-}/[\text{Ni}(\text{dmit})_2]^0/[\text{Ni}(\text{dmit})_2]^{1-}$  sandwich in which two anions are related to each other through an inversion center (**Figure 2c**). The  $[\text{Ni}(\text{dmit})_2]^-$  anions located between neighboring trimers are arranged into a two-legged ladder chain *via* shorter lateral to lateral S $\cdots$ S bonding interactions along the crystallographic  $a$ - and  $b$ -axes (**Figure 2d**). The neutral  $[\text{Ni}(\text{dmit})_2]^0$  species between adjacent trimers form a one-dimensional straight chain through head to tail S $\cdots$ S bonding interactions along the crystallographic  $b$ -axis direction within the mixed-valence  $[\text{Ni}(\text{dmit})_2]$  molecule layer (**Figure 2e**). The short interatomic distances are less than the sum of van der Waals radii of two S atoms (3.7 Å) and are listed below:  $d_{\text{S}(4)\cdots\text{S}(9)\#1} = 3.619(1)$ ,  $d_{\text{S}(2)\cdots\text{S}(2)\#1} = 3.480(1)$ ,  $d_{\text{S}(6)\cdots\text{S}(8)\#2} = 3.461(1)$  and  $d_{\text{S}(6)\cdots\text{S}(10)\#2} = 3.450(1)$  Å within a ladder chain;  $d_{\text{S}(13)\cdots\text{S}(13)\#3} = 3.469(1)$  Å within a  $[\text{Ni}(\text{dmit})_2]^0$  chain and  $d_{\text{Ni}(2)\cdots\text{S}(1)\#4} = 3.561(1)$  and  $d_{\text{Ni}(1)\#4\cdots\text{S}(12)} = 3.588(1)$  Å between the longitudinal offset  $[\text{Ni}(\text{dmit})_2]^0$

and  $[\text{Ni}(\text{dmit})_2]^{1-}$  species (symmetric codes #1 =  $1 - x, -y, 1 - z$ ; #2 =  $x, -1 + y, z$ ; #3 =  $-x, 1 - y, 1 - z$  and #4 =  $x, 1 + y, z$ ).

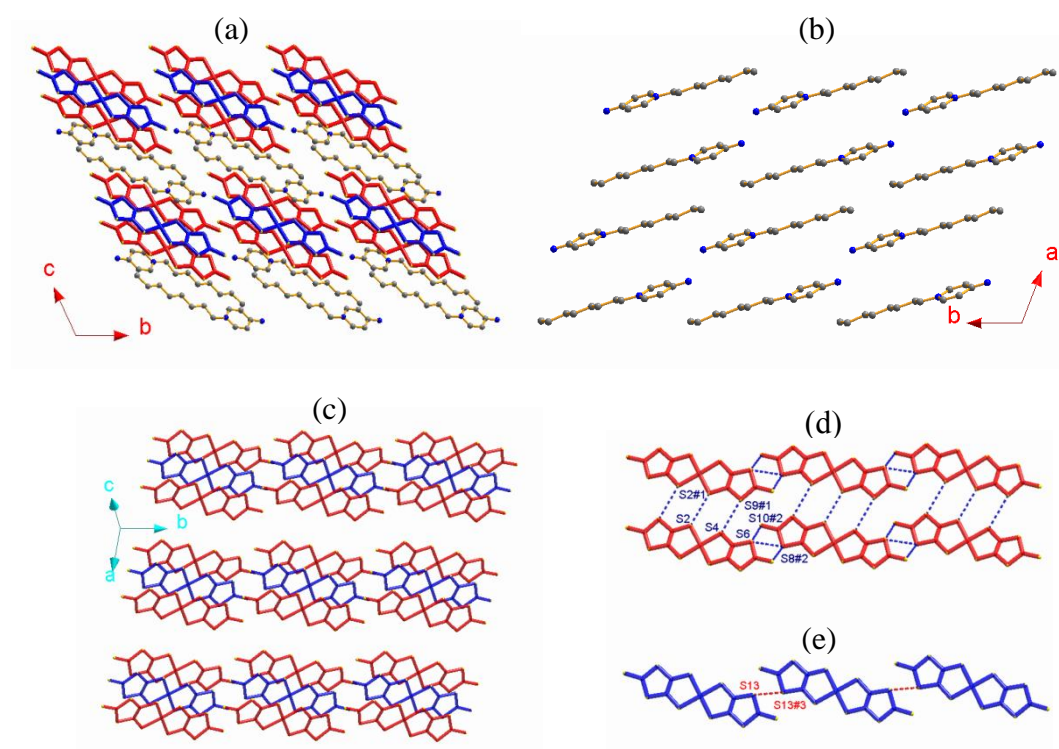


**Figure 2** (a) Alternating layers of  $\text{C}_8\text{-APy}^+$  cations (H atoms are omitted for clarity) and mixed-valence  $[\text{Ni}(\text{dmit})_2]$  species (where blue = neutral species and red = anionic species) viewed along the crystallographic  $a$ -axis in compound **1**; (b) the cationic layer; (c) the  $[\text{Ni}(\text{dmit})_2]$  species layer; (d) the two-legged  $[\text{Ni}(\text{dmit})_2]^{1-}$  ladder chain and (e) the one-dimensional  $[\text{Ni}(\text{dmit})_2]^0$  chain (where the dotted lines represent  $\text{S}\cdots\text{S}$  bonding interactions  $< 3.7 \text{ \AA}$ ).

### Relationship of magnetic property and structure

The magnetic susceptibility ( $\chi_m$ ) of compound **1** as a function of temperature (in a range of 1.8–400 K) is shown in **Figure 3**. A broad maximum centered at  $\sim 120 \text{ K}$ , followed by an exponential drop is observed in the  $\chi_m$ -T curve upon cooling, indicating the existence of a gap in the spin excitation spectrum and is characteristic of a low-dimensional AFM exchange system. In addition, the Curie–Weiss type magnetic behavior dominates in the low temperature region ( $< 20 \text{ K}$ ).

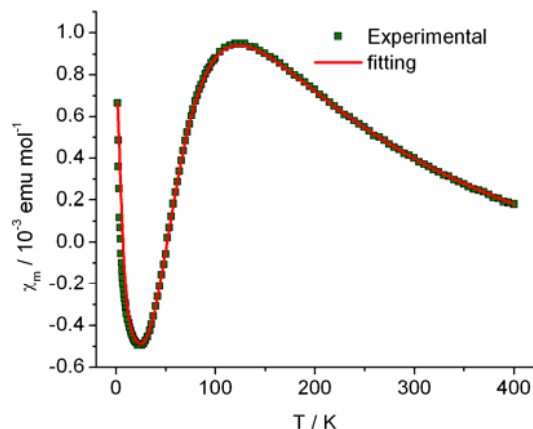


**Figure 3** Temperature dependence of the molar magnetic susceptibility ( $\chi_m$ ) with one  $[\text{Ni}(\text{dmit})_2]^{1-}$  species per formula unit in compound **1** (where solid line = fit plot and open circles = experimental data).

To understand the magnetic coupling between neighboring  $[\text{Ni}(\text{dmit})_2]^-$  anions in compound **1**, a broken symmetry DFT approach<sup>22</sup> was employed to evaluate the magnetic coupling constants.

The magnetic coupling between neighboring  $[\text{Ni}(\text{dmit})_2]^-$  anions can be transmitted through non-bonding interactions, especially through S atoms, due to the delocalization of the unpaired electron over the whole skeleton of the  $[\text{Ni}(\text{dmit})_2]^-$  anion. Using the X-ray crystal structure analysis (Figure 2c and 2d), three types of magnetic couplings were identified, one within the trimer with the magnetic coupling constant  $J_1$  and the other two within the two-legged ladder chain, with the magnetic coupling constant  $J_2$  corresponding to the ladder rung and  $J_3$  the ladder rail direction.

The  $\langle S^2 \rangle_{\text{HS}}$ ,  $\langle S^2 \rangle_{\text{BS}}$  and  $J$  values for compound **1** were calculated using Equations 2–4 (see the ESI) and are summarized in Table 2. These results show: (1) a strong AFM interaction exists within a trimer, a weak AFM interaction along the rail direction and a negligible magnetic coupling along the rung direction within the two-legged ladder chains is observed. This indicates that the magnetic behavior of compound **1** is dominated by the magnetic coupling within the trimer. (2) The calculated  $\langle S^2 \rangle_{\text{HS}}$  values in the three types of magnetic couplings are close to the

angular momentum eigenvalue found in the high-spin triplet state,  $S_T(S_T+1) = 1(1+1) = 2$ , whilst the calculated  $\langle S^2 \rangle_{BS}$  values for  $J_1$  (1.1294),  $J_2$  (1.0096) and  $J_3$  (1.0091) show relatively high spin contamination. (3) The calculated magnetic coupling constants, using Equations S2 and S4 (see the ESI), are similar to each other demonstrating the existence of ‘weak bonding’ within the spin dimer. The frontier molecular orbitals of the BS states of  $J_1$  and  $J_3$ , indicate the existence of a partial overlap between the two SOMOs within the sandwich trimer and spin localized in an individual  $[\text{Ni}(\text{dmit})_2]^-$  anion for the magnetic exchange pathway of  $J_3$  (Figure 4). In combination with the spin density distribution analysis, we can conclude that the magnetic couplings between the neighboring  $[\text{Ni}(\text{dmit})_2]^-$  anions are achieved through orbital overlap together with a weak spin polarization mechanism within the sandwich trimer. In addition, only a spin polarization mechanism is observed for the ladder chain along the rail direction in compound **1**.

**Table 2** Calculated  $\langle S^2 \rangle_{HS}$  and  $\langle S^2 \rangle_{BS}$  and  $J$  values for each magnetic coupling pathway in compound **1**

Coupling pathway	$J_1/k_B$ (K)	$J_2/k_B$ (K)	$J_3/k_B$ (K)	$\langle S^2 \rangle_{HS}$	$\langle S^2 \rangle_{BS}$
$J_1$ (within a trimer)	-96.8	-48.4	-109.5	2.0134	1.1294
$J_2$ (along ladder rung)	0.098	0.049	0.098	2.0097	1.0096
$J_3$ (along ladder rail)	-1.8	-0.9	-1.8	2.0095	1.0091

Notes:  $J_1/k_B$ ,  $J_2/k_B$  and  $J_3/k_B$  were obtained using Equations 2–4 (see the ESI).

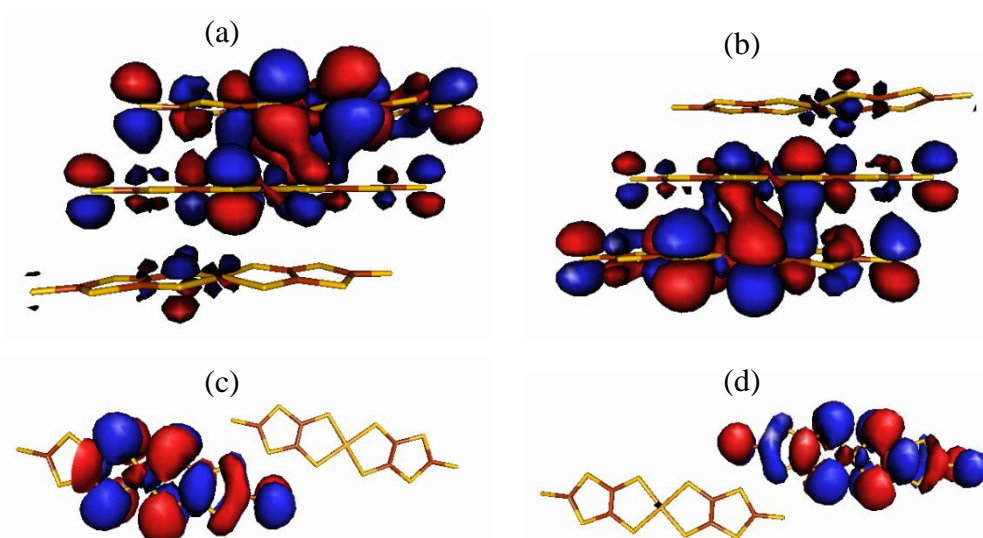


**Figure 4** SOMOs in the BS states for  $J_1$  (a, b) and  $J_3$  (c, d), respectively.

On the basis of the analysis described beforehand, a simple  $S = 1/2$  spin dimer model was chosen to fit the magnetic susceptibility over the whole temperature range. In addition, to take into account the Curie–Weiss and temperature independent magnetic susceptibilities, the experimental molar magnetic susceptibility is expressed in Equation 1.

$$\chi_m = \frac{Ng^2\mu_B^2}{k_B T} \frac{1}{3 + \exp(2J/k_B T)} + \frac{C}{T - \theta} + \chi_0 \quad (\text{Equation 1})$$

In Equation 1, the first term represents the magnetic susceptibility contribution from a spin dimer with two  $S = 1/2$  monomers, deduced from spin Hamiltonian  $\mathbf{H} = -2\mathbf{S}_1\mathbf{S}_2$  and  $J$  is the intra dimer magnetic coupling constant. The  $C/(T-\theta)$  term arises from the magnetic impurity and  $\chi_0$  is the sum of diamagnetism and possible van Vleck paramagnetism related to the coupling of ground and excited states *via* a magnetic field.<sup>23</sup> The  $\chi_m$ - $T$  plot in the temperature range 1.8–400 K (**Figure 3**) was reproduced using Equation 1 with the parameters:  $J/k_B = -99.7(0)$  K (corresponding  $\Delta/k_B = 199.4$  K),  $\chi_0 = -6.8(2) \times 10^{-4}$  emu mol<sup>-1</sup>,  $C = 4.03(3) \times 10^{-3}$  emu K mol<sup>-1</sup> and  $\theta = -1.19(3)$  K with a  $g$ -factor = 2.045(1). The fitted  $J$  value is close to the calculated  $J_1$  value. In addition, on the basis of the fitted Curie constant, the amount of  $S = 1/2$  magnetic impurities were estimated to be ~1.1%.

### Conductivity and photoconductivity

Compound **1** displays semi-conductor character, the  $\sigma = 1.5 \times 10^{-6}$  S cm<sup>-1</sup> at 303 K (30 °C) as shown in **Figure 5a**. The activation energy was estimated to be 0.33 eV by fitting the variable temperature conductivity in the temperature range of 300–420 K using the Arrhenius equation (Equation 2).

$$\sigma = \sigma_0 \exp\left(\frac{E_a}{k_B T}\right) \quad (\text{Equation 2})$$

The photoconductivity for compound **1** was investigated and the photocurrent monitored as a function of time with an alternating ON and OFF UV irradiation (Figure 5b). After a few seconds of irradiation, the current increases sharply, to reach a saturation value. The relaxation back to the original dark current was observed after switching off the illumination.

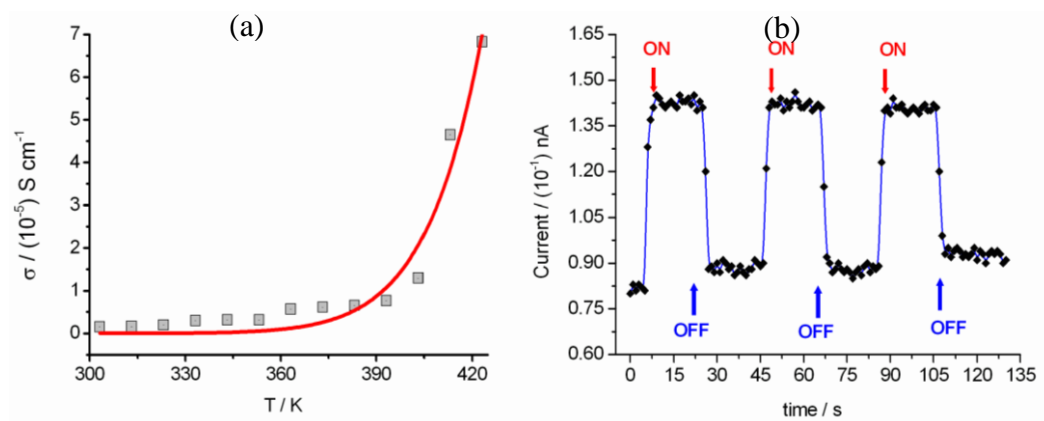


**Figure 5** (a) Plot of electrical conductivity ( $\sigma$ ) of compound **1** versus temperature from 303–423 K (Red line = theoretically produced plot using Equation 2). (b) The photocurrent  $I$  response to UV irradiation ( $\lambda_{UV} = 375$  nm; 3.3 eV) was measured using a needle-shaped single crystal at 300 K with the applied voltage = 0.1 V and light intensity =  $45 \text{ mW}\cdot\text{cm}^{-2}$ , and two gold wires with a diameter of 80  $\mu\text{m}$  were attached on two opposite surfaces of the cross section of needle crystal.

For photoconductivity, several different mechanisms have been reported to occur in  $[\text{M}(\text{dmit})_2]$  ( $\text{M} = \text{Ni}$  or  $\text{Pd}$ ) molecular solids. Ishikawa and co-workers<sup>24</sup> reported the compounds  $\text{Et}_2\text{Me}_2\text{Sb}[\text{Pd}(\text{dmit})_2]_2$  and  $\text{Cs}[\text{Pd}(\text{dmit})_2]_2$  that display ultrafast photoconductive response. These molecular solids possess two different crystalline phases with distinct conductivity and their photoinduced phase transition leads to the ultrafast photoconductive response. Naito and co-workers<sup>9</sup> reported a novel charge-transfer (CT) photoconductor,  $\text{BPY}[\text{Ni}(\text{dmit})_2]_2$  (where;  $\text{BPY} = N, N'$ -ethylene-2, 2'-bipyridinium), in which the molecular orbitals of  $\text{BPY}^{2+}$  and  $[\text{Ni}(\text{dmit})_2]^-$  mix to form energy bands. The interband transitions occur in the UV spectroscopic region corresponding to the CT bands between  $\text{BPY}^{2+}$  and  $[\text{Ni}(\text{dmit})_2]^-$ ,

generating new carriers of holes and electrons and is responsive to the photoconductivity of BPY[Ni(dmit)<sub>2</sub>]<sub>2</sub>. On the basis of the variable temperature magnetic susceptibility measurements (Figure 3) and the DSC analysis over the temperature range of 293–473 K, no phase transition was observed for compound **1**. Therefore, a photoinduced phase transition mechanism for photoconductivity can be excluded for compound **1**.

The energy band structures for the two-dimensional, mixed valence layer in compound **1** were analyzed and the calculated bands along the high symmetry directions of the Brillouin zone are shown in Figure 6. The valence band (VB) was observed near the Fermi level and a small dispersion along the *c*-axis (approximately from G to Z in k-space) indicative of weak bonding interactions between the mixed valence layers and the two-dimensional electronic nature of this molecular solid. These results are in agreement with the X-ray crystal structure analysis in which neighboring mixed valence layers are separated by a cationic layer. The VB is relatively sharp along the direction from G to Y in the k-space, indicating the existence of stronger bonding interactions in the mixed valence layer. The calculated energy gap between the highest occupied and the lowest unoccupied bands is 0.519 eV, a value almost double that obtained from the conductivity measurements and attributed to the limitations of DFT methods.<sup>25</sup> The orbitals of the [Ni(dmit)<sub>2</sub>]<sup>−</sup> and [Ni(dmit)<sub>2</sub>]<sup>0</sup> species mix to form energy bands in compound **1** and the photoconductivity of **1** arising due to interband transitions in the UV spectroscopic region corresponding to the CT bands between the [Ni(dmit)<sub>2</sub>]<sup>−</sup> and [Ni(dmit)<sub>2</sub>]<sup>0</sup> species. However, further investigation is needed to understand the novel photoconductivity of compound **1** (Figure 6a).

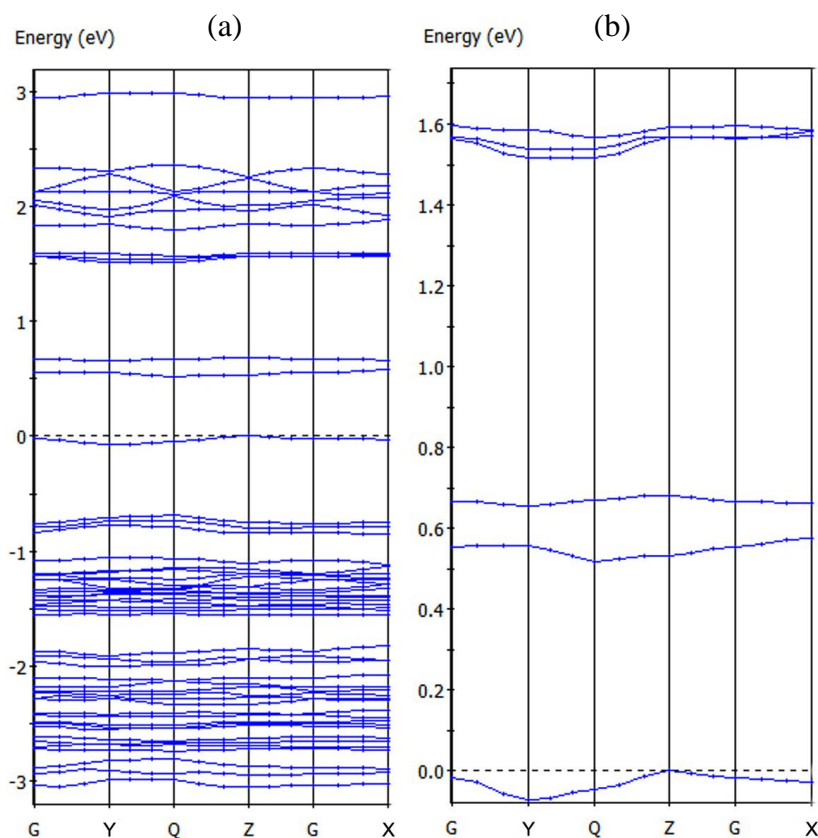


**Figure 6** (a) Dispersion relations of the mixed valence layer in compound **1** [where; Fermi levels are shown by dashed lines and the k-points: G = (0, 0, 0), X = (0.5, 0, 0), Y = (0, 0.5, 0), Z = (0, 0, 0.5) and Q = (0, 0.5, 0.5)]. (b) Magnified view of the highest occupied band and several lowest unoccupied bands.

## Conclusion

In summary, a novel, two-dimensional, mixed-valence  $[\text{Ni}(\text{dmit})_2]$  compound,  $[\text{C}_8\text{-Apy}]_2[\text{Ni}(\text{dmit})_2]_3$  (**1**) has been prepared possessing an unusual 2:3 stoichiometry between the monocation  $\text{C}_8\text{-Apy}^+$  and  $[\text{Ni}(\text{dmit})_2]$  species. The  $[\text{Ni}(\text{dmit})_2]$  layer is constructed from alternating straight chains of  $[\text{Ni}(\text{dmit})_2]^0$  and two-legged ladder chains of  $[\text{Ni}(\text{dmit})_2]^{1-}$ . Compound **1** displays semi-conductor character and AFM dimer magnetic behavior in addition to a rapid, clear and stable response of photoconductivity under UV irradiation. The magnetic coupling nature was analyzed using the ‘broken-symmetry’ DFT approach and the novel photoconductivity attributed to the electronic transitions between the  $[\text{Ni}(\text{dmit})_2]^{1-}$  and  $[\text{Ni}(\text{dmit})_2]^0$

species in **1**. This work suggests mixed-valence  $[\text{Ni}(\text{dmit})_2]$  compounds have great potential as the building blocks for new photoconductor based materials.

### Supporting Information

Electronic Supplementary Information (ESI) available: Details of broken-symmetry DFT approach, average bond lengths, the characteristic vibration frequencies ( $\text{cm}^{-1}$ ) for  $[\text{Ni}(\text{dmit})_2]^{n-}$  ( $n = 0, 1$ ), calculated overlap and transfer integrals for each spin dimer in the two-legged ladder chain of **1**. Figures include IR spectrum, TG, DTA and PXRD Profiles. See DOI: 10.1039/b000000x/

### Acknowledgments

The authors would like to thank the Priority Academic Program Development of Jiangsu Higher Education Institutions and the National Nature Science Foundation of China (Grant nos. 91122011, 21071080 and 21271103) for financial support.

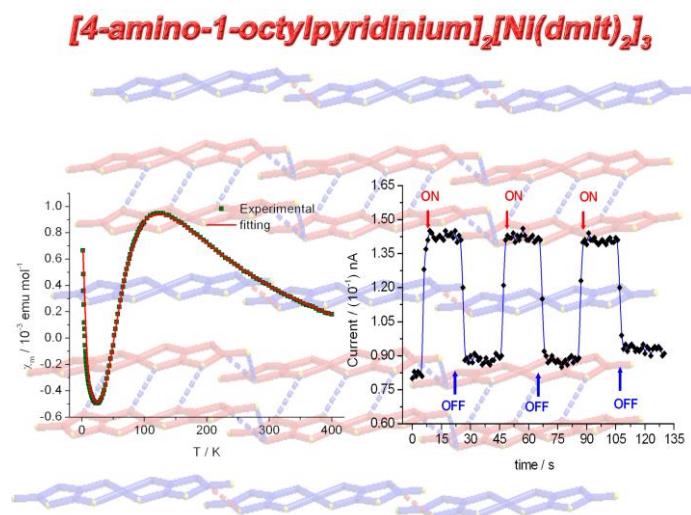
## Notes and references

1. R. Kato, *Chem. Rev.*, 2004, **104**, 5319; K. Kanoda and R. Kato, *Annu. Rev. Condens. Matter Phys.*, 2011, **2**, 167; T. Kusamoto, H. M. Yamamoto, N. Tajima, Y. Oshima, S. Yamashita and R. Kato, *Inorg. Chem.*, 2012, **51**, 11645.
2. T. Nakamura, T. Akutagawa, K. Honda, A. E. Underhill, A. T. Coomber and R. H. Friend, *Nature*, 1998, 394, 159; T. Akutagawa, H. Koshinaka, D. Sato, S. Takeda, S.-I. Noro, H. Takahashi, R. Kumai, Y. Tokura and T. Nakamura, *Nat. Mater.*, 2009, **8**, 342.
3. T. Kusamoto, H. M. Yamamoto, N. Tajima, Y. Oshima, S. Yamashita and R. Kato, *Inorg. Chem.*, 2013, **52**, 4759.
4. J. Lieffrig, O. Jeannin, P. Auban-Senzier and M. Fourmigué, *Inorg. Chem.*, 2012, **51**, 7144.
5. Y. K. Han, D. K. Seo, H. Kang, W. Kang and D. Y. Noh, *Inorg. Chem.*, 2004, **43**, 7294; D. Y. Noh, A. E. Underhill and M. B. Hursthouse, *Synth. Met.*, 2001, **120**, 1053; D. Y. Noh, H. J. Lee, H. Kang, W. Kang and U. Lee, *Mol. Cryst. Liq. Cryst.*, 2002, **376**, 269.
6. P. Cassoux, L. Valade, H. Kobayashi, A. Kobayashi, R. A. Clark and A. E. Underhill, *Coord. Chem. Rev.*, 1991, **110**, 115.
7. A. E. Pullen and R.-K. Olk, *Coord. Chem. Rev.*, 1999, **188**, 211.
8. M. Bousseau, L. Valade, J. Legros, P. Cassoux, M. Garbauskas and L. V. Interrante, *J. Am. Chem. Soc.*, 1986, **108**, 1908.
9. T. Naito, T. Karasudani, S. Mori, K. Ohara, K. Konishi, T. Takano, Y. Takahashi, T. Inabe, S. Nishihara and K. Inoue, *J. Am. Chem. Soc.*, 2012, **134**, 18656.
10. Q. H. Li, T. Gao, Y. G. Wang and T. H. Wang, *Appl. Phys. Lett.*, 2005, **86**, 123117; T. Y. Wei, C. T. Huang, B. Hansen, Y. F. Lin, L. J. Chen, S. Y. Lu and Z. L. Wang, *Appl. Phys. Lett.*, 2010, **96**, 013508.
11. G. Steimecke, H.-J. Sieler, R. Kirmse and E. Hoyer, *Phosphorous Sulfur*, 1979, **7**, 49.

12. H. B. Duan, X. M. Ren, L. J. Shen, W. Q. Jin, Q. J. Meng, Z. F. Tian and S. M. Zhou, *Dalton Trans.*, 2011, **40**, 3622.
13. G. M. Sheldrick, *SADABS*, Program for Bruker Area Detector Absorption Correction, University of Göttingen, Göttingen, Germany, 1997.
14. G. M. Sheldrick, *SHELXS-97*, Program for Crystal Structure Solution, University of Göttingen, Göttingen, Germany, 1997.
15. M. J. Frisch, G. W. Trucks, H. B. Schlegel, et al., *Gaussian 09*, Revision **A.02**, Gaussian, Inc., Wallingford CT, 2009.
16. A. D. Becke, *J. Chem. Phys.*, 1993, **98**, 5648.
17. W. Y. C. Lee and R. G. Parr, *Phys. Rev. B*, 1988, **37**, 785.
18. T. H. Dunning Jr. and P. J. Hay, *Modern Theoretical Chemistry*, Plenum, New York, 1976, p. 1-28; P. J. Hay and W. R. Wadt, *J. Chem. Phys.*, 1985, **82**, 270; W. R. Wadt and P. J. Hay, *J. Chem. Phys.*, 1985, **82**, 284; P. J. Hay and W. R. Wadt, *J. Chem. Phys.*, 1985, **82**, 299.
19. M. D. Segall, P. J. D. Lindan, M. J. Probert, C. J. Pickard, P. J. Hasnip, S. J. Clark and M. C. Payne, *J. Phys.: Condens. Matter*, 2002, **14**, 2717; V. Milman, B. Winkler, J. A. White, C. J. Pickard, M. C. Payne, E. V. Akhmatkaya and R. H. Nobes, *Int. J. Quantum Chem.* 2000, **77**, 895.
20. J. P. Perdew, K. Burke and M. Ernzerhof, *Phys. Rev. Lett.*, 1996, **77**, 3865.
21. H. J. Monkhorst and J. D. Pack, *Phys. Rev. B.*, 1976, **13**, 5188.
22. L. Noodleman and J. G. Jr. Norman, *J. Chem. Phys.*, 1979, **70**, 4903.
23. J. H. Van Vleck, *The theory of electric and magnetic susceptibilities*, Oxford University Press, Oxford, U. K., 1932.
24. T. Ishikawa, N. Fukazawa, Y. Matsubara, R. Nakajima, K. Onda, Y. Okimoto, S. Koshihara, M. Lorenc, E. Collet, M. Tamura and R. Kato, *Phys. Rev. B*, 2009, **80**, 115108; N. Fukazawa, T. Tanaka, T. Ishikawa, Y. Okimoto, S. Koshihara, T. Yamamoto, M. Tamura, R. Kato, K. Onda, *J. Phys. Chem. C*, 2013, **117**, 13187.

25. R. W. Godby, M. Schluther and L. Sham, *J. Phys. Rev. B*, 1987, **36**, 6497; C. M. I. Okoye, *J. Phys.: Condens. Matter*, 2003, **15**, 5945; R. Terki, G. Bertrand and H. Aourag, *Microelectron. Eng.*, 2005, **81**, 514.

## TOC



A novel, two-dimensional mixed-valence [Ni(dmit)<sub>2</sub>] molecular solid shows a rapid, clear and stable response of photoconductivity under UV irradiation.